

Sustainedly High-Rate Electroreduction of CO₂ to Multi-Carbon Products on Nickel Oxygenate/Copper Interfacial Catalysts

Xuejiao Mao, Chun-Wai Chang, Zhiguo Li, Zishan Han, Jiachen Gao, Mason Lyons, George Sterbinsky, Yong Guo, Bo Zhang, Yaogang Wang, Xinyu Wang, Daliang Han, Quan-Hong Yang, Zhenxing Feng,* and Zhe Weng*

Copper (Cu) is the most attractive electrocatalyst for CO_2 reduction to multi-carbon (C_{2+}) products with high economic value in considerable amounts. However, the rational design of a structurally stable Cu-based catalyst that can achieve high activity and stability towards C_{2+} products remain a grand challenge. Here, a highly stable nickel oxygenate/Cu electrocatalyst is developed with abundant NiOOH/Cu interfaces by in situ electrochemical reconstruction. The nickel oxygenate/Cu electrocatalyst achieves a superior Faradaic efficiency of $86.3 \pm 3.0\%$ and a record partial current density of 2085 A g $^{-1}$ for C_{2+} products with long-term stability. In situ experimental and theoretical studies demonstrates that the exceptional performance in generating C_{2+} products is attributed to the presence of the NiOOH/Cu interfaces which increase *CO coverage, lower energy barrier for *CO coupling and stabilize *OCCO simultaneously. This work provides new insights into the rational design of electrocatalysts to achieve stable and efficient electrocatalytic CO_2 reduction capabilities.

1. Introduction

Carbon dioxide (CO_2) in the atmosphere gradually increasing has led to severe environmental issues, such as global warming. Electrochemical CO_2 reduction reaction (CO_2RR) driven by renewable energy is a promising strategy to mitigate climate deterioration and close the carbon cycle. Among numerous products formed by CO_2RR , multi-carbon (C_{2+}) products are

desirable because of their high energy density and economic values. [3] Copper (Cu) is the most attractive electrocatalyst for $\mathrm{CO_2RR}$ that can produce $\mathrm{C_{2+}}$ products in considerable amounts. [4] Although significant progress has been achieved, Cu electrocatalysts still struggle to achieve high $\mathrm{C_{2+}}$ selectivity and activity at industrial current densities due to the sluggish kinetics of the C—C coupling step. [4–5]

Recent studies reported that bimetallic electrocatalysts exhibit improved C₂₊ selectivity and activity compared to pure Cu.^[6] The enhanced C—C coupling step on bimetallic electrocatalysts is attributed to the stabilization of key intermediates, such as *CO and *OCCO, through unique electronic structure, strain effect, or geometric effects introduced by the secondary metal.^[7] Among the numerous metallic elements, nickel (Ni) is

considered a promising candidate due to its strong affinity for oxygen, which can potentially stabilize O-containing intermediates. Therefore, several Cu—Ni bimetallic electrocatalysts have been developed to promote the formation of C_{2+} products. Unfortunately, like other bimetallic electrocatalysts, their structural instability poses a significant challenge. Under the conditions of CO_2 reduction, these electrocatalysts tend to undergo electrochemical reconstruction, leading to

X. Mao, Z. Li, Z. Han, J. Gao, Y. Guo, B. Zhang, Y. Wang, X. Wang, D. Han, Q.-H. Yang, Z. Weng

Nanoyang Group, Tianjin Key Laboratory of Advanced Carbon and Electrochemical Energy Storage, School of Chemical Engineering and Technology, and Collaborative Innovation Center of Chemical Science and Engineering (Tianjin)

Tianjin University
Tianjin 300072, China
E-mail: zweng@tju.edu.cn

X. Mao, Z. Li, Z. Han, J. Gao, Y. Guo, B. Zhang, Y. Wang, X. Wang, D. Han, Q.-H. Yang, Z. Weng

National Industry-Education Integration Platform of Energy Storage Tianjin University

Tianjin 300072, China

DOI: 10.1002/aenm.202400827

X. Mao, Z. Li, Z. Han, J. Gao, Y. Guo, B. Zhang, Y. Wang, X. Wang, D. Han, Q.-H. Yang, Z. Weng

Haihe Laboratory of Sustainable Chemical Transformations Tianjin 300192, China

C.-W. Chang, M. Lyons, Z. Feng

School of Chemical, Biological, and Environmental Engineering Oregon State University

Corvallis, OR 97331, USA

E-mail: zhenxing.feng@oregonstate.edu

G. Sterbinsky Advanced Photon Source Argonne National Laboratory Argonne, IL 60439, USA

1614680, 2024, 25, Downloaded from https://dvanced.onlineb.trary.wiley.com/do/i01.0102/denm.20240827 by Zhenxing Feng - Organ State University, Wiley Online Library on (07/07/2025], See the Terms and Conditions (https://onlinebtrary.wiley.com/ems-and-conditions) on Wiley Online Library for rules of use; OA articles are governed by the applicable Creative Commons Licenses

www.advancedsciencenews.com

www.advenergymat.de

uncontrollable selectivity and activity of CO_2RR . [9,10] For example, the Cu—Ni bimetallic electrocatalysts often demonstrate Ni segregation, which causes an unwanted hydrogen evolution reaction (HER). [9a] Thus, it is crucial to construct structurally stable Cu—Ni electrocatalysts for achieving sustainedly high selectivity and activity of CO_2RR to C_{2+} products.

Considering the excellent structural stability and strong binding ability to O-containing intermediates, [11] here we explored using nickel oxygenates ($Ni^{\delta+}$ species) as an alternative to metallic Ni atoms, and successfully in situ constructed a nickel oxide hydroxide (NiOOH)/Cu electrocatalyst with abundant NiOOH/Cu interfaces during CO₂RR. In situ X-ray absorption spectroscopy (XAS) and in situ surface-enhanced Raman spectra results verified that the NiOOH/Cu interfacial structure keeps stable during CO₂RR and significantly increases the adsorption of *CO compared to the pure Cu surface. Theoretical calculations demonstrated that the NiOOH/Cu interfaces also provide dual sites for stabilizing *OCCO intermediates and decrease the kinetic barrier for C-C coupling. As a result, the NiOOH/Cu electrocatalyst shows an impressive C_{2+} Faradaic efficiency (FE) of 86.3 \pm 3.0% at an industrial current density of 400 mA cm⁻². The selectivity of C₂H₄ maintains above 50% with high stability over 5 h. More intriguingly, the NiOOH/Cu interfaces exhibit extremely high electrocatalytic activity toward C2+ products with a recorded partial current density of 2085 A g⁻¹.

2. Results and Discussion

The NiOOH/Cu electrocatalyst was synthesized in two steps (Figure 1a). In the first step, Ni—Cu oxygenate precursor (NiCu-OP) was prepared by an epoxide gel approach, forming a uniform sol-gel (Figure S1, Supporting Information). The powder X-ray diffraction (XRD) pattern of the NiCu-OP was found to be almost identical to that of pure Cu₂(OH)₃Cl (Figure S2, Supporting Information), which is consistent with literature results that Ni species doping does not significantly change the lattice parameters of Cu₂(OH)₃Cl.^[12] X-ray photoelectron spectroscopy (XPS) confirmed that Cu and Ni coexist in the material, and they are in the 2+ and 3+ oxidation states, respectively (Figure S3, Supporting Information). Scanning electron microscopy (SEM) and highresolution transmission electron microscopy (HR-TEM) images displayed that the NiCu-OP has a microporous structure composed of aggregated nanoclusters (Figures S4 and S5, Supporting Information). The energy-dispersive X-ray spectroscopy (EDS) mapping reveals that Cu and Ni elements are uniformly distributed over the whole gel framework (Figure S6, Supporting Information).

In the second step, the NiCu-OP powders were mixed with solvents and binders to prepare ink, and then the ink was applied onto carbon paper, forming Ni—Cu electrodes, which were subsequently assembled into a flow cell. The NiOOH/Cu electrocatalyst was in situ obtained by electrochemical reduction of the Ni—Cu electrode under a constant current density of -100 mA cm^{-2} in 1 m KOH electrolyte for 30 min. After this treatment, numerous nanoparticles are presented with an average diameter of 10–30 nm on the carbon paper (Figures 1b; Figure S7, Supporting Information). The XRD pattern shows a metallic Cu crystal structure and an amorphous β -NiOOH structure (Figure S2, Supporting Information). In the HR-TEM

images (Figure 1c,d), lattice fringes with dimensions of 0.241 and 0.208 nm correspond to the NiOOH (001) and Cu (111) lattice planes, respectively,[13] which confirms the presence of NiOOH/Cu interfaces. The EDS mapping images show a clear phase separation between Ni and Cu on a microscale (Figure 1e), but the Large-scale ones exhibit a uniform dispersion of Ni and Cu elements (Figure S8, Supporting Information), which indicates that there are a large number of NiOOH/Cu interfaces uniformly dispersed in the NiOOH/Cu electrocatalyst. XPS measurements were then performed to characterize the surface chemical compositions and oxidation states. The Ni 2p_{3/2} peaks at the binding energies of 856.4 and 855.2 eV are attributed to Ni (III) and Ni(II), respectively (Figure 1f).[14] The average valence state of Ni is 2.7+, indicating that NiOOH was only slightly reduced in the NiOOH/Cu electrocatalyst. The Cu 2p_{3/2} peak at a binding energy of 932.28 eV is attributed to Cu (0), supporting the existence of metallic Cu (Figure 1g). Another peak at 933.08 eV attributed to Cu (II) should result from the slight oxidation of metallic Cu in air. Overall, the NiOOH/Cu electrocatalyst with abundant interfaces was in situ generated by electroreduction.

To gain further insights into the structure and oxidation state changes of the NiOOH/Cu electrocatalyst during in situ construction, we carried out in situ XAS measurements (Figure 2; Figures S9 and S10, Supporting Information).[15] The applied potential was gradually decreased in steps from the open circuit voltage (OCV, \approx 0.8 V versus RHE) to -1.4 V versus RHE during the measurements. Under all working potentials, the catalyst showed a characteristic Ni(III) peak at the edge position, ≈8,343 eV, in the corresponding normalized Ni K-edge X-ray absorption near-edge structure (XANES) spectrum (Figure 2a). When the reduction potential was applied, the edge position moved to the lower energy region, indicating an oxidation state of Ni decreased slightly (Table S1, Supporting Information), aligning with the findings from XPS (Figure 1f). The k3-weighted Fourier-transformed extended X-ray absorption fine structure (EXAFS) spectra displayed a characteristic Ni–O bond peak at $R = \approx 1.56$ Å and Ni–Ni bond peak at $R = \approx 2.76$ Å at all working potentials (Figure 2b), which demonstrates that Ni species exist in a NiOOH structure under all conditions. These results illustrate that the oxidation state and structure of Ni are maintained during the in situ formation process of the NiOOH/Cu electrocatalyst. In the meantime, the ratio of the Ni-O scattering peak to the Ni-Ni scattering peak was reduced as the reduction potentials were decreased from OCV to -1.4 V (Table S2, Supporting Information), which is likely indicative of the formation of oxygen vacancies from NiOOH consistent with the trend of XANES.

Under the initial OCV condition, the NiCu-OP exhibits a characteristic Cu (II) peak at $\approx 8,985$ eV in the corresponding normalized Cu K-edge XANES spectra (Figure 2c). As the potential was decreased to -0.8 V, a peak at $\approx 8,980$ eV corresponding to Cu (0) was presented, which validates the XRD result (Figure S2, Supporting Information). Within the range of -0.8 V to -1.4 V, the stable retention of Cu (0) indicates the conversion of nearly all Cu (II) centers to lower oxidation states under low potential conditions, in line with literature results that $\text{Cu}_2(\text{OH})_3\text{Cl}$ will be reduced to a metallic Cu at a negative potential. In the Cu K-edge EXAFS spectra (Figure 2d), the NiOOH/Cu electrocatalyst displayed a distinctive metallic Cu—Cu bond peak at 2.48 Å from -0.8 to -1.4 V, which shows the metallic nature of Cu

161 46840, 2024, 25, Downloaded from https://advanced.onlinelibrary.wiley.com/doi/10.1002/nerm.202400827 by Zhenxing Feng - Oregon State University , Wiley Online Library on [0707/2025]. See the Terms and Conditions (https://oinelibrary.

) on Wiley Online Library for rules of use; OA articles are governed by the applicable Creative Commons

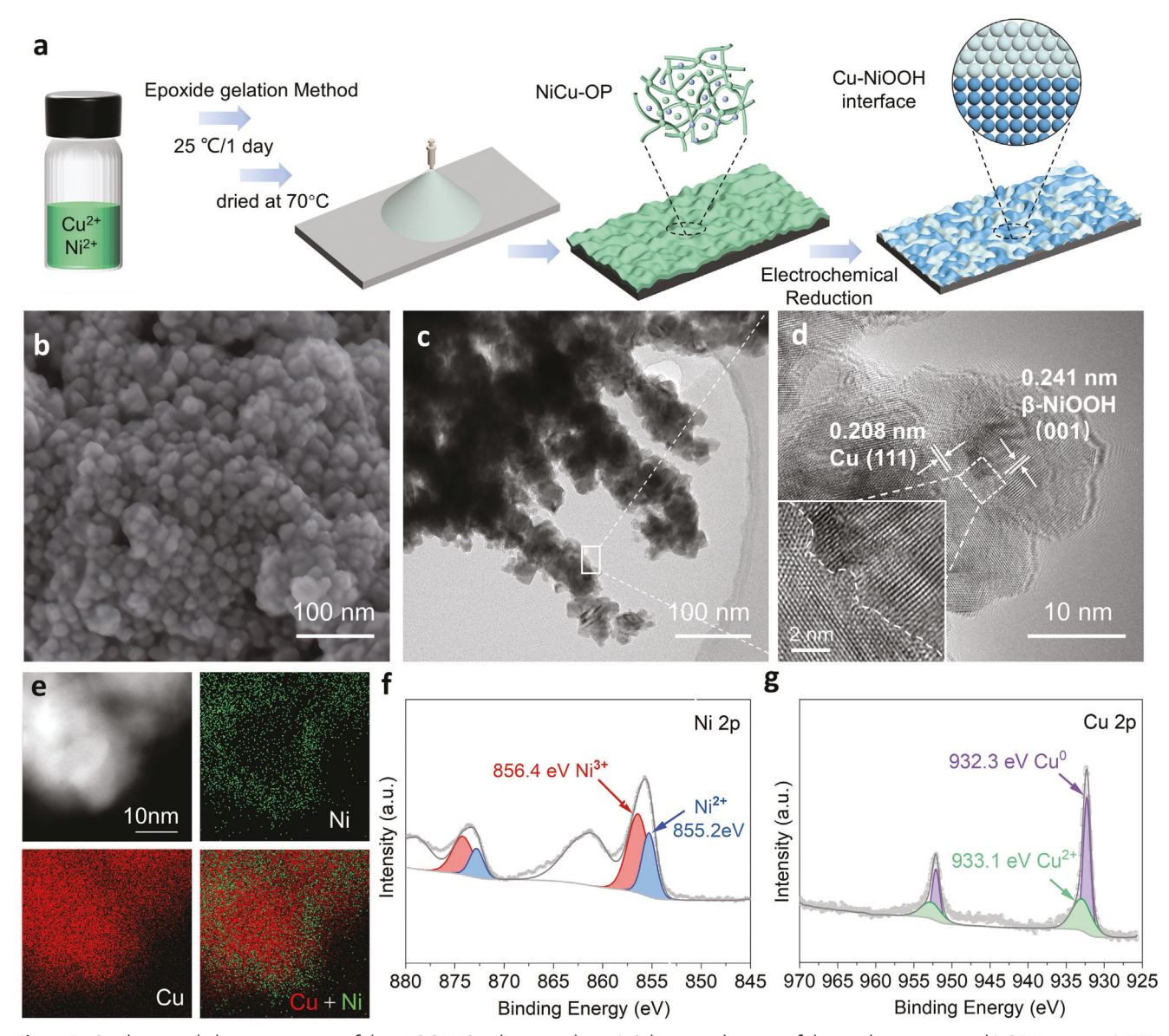


Figure 1. Synthesis and characterizations of the NiOOH/Cu electrocatalyst. a) Schematic diagram of the synthesis process. b) SEM image, c) TEM image, d) HR-TEM image, and the corresponding e) EDS mapping, f,g) XPS spectra of Ni 2p and Cu 2p.

active sites, consistent with the observation of Cu (0) in the XANES spectra. [15c] The above XAS results and microstructural characterizations illustrate that $\mathrm{Cu_2(OH)_3Cl}$ was reduced to metallic Cu nanoparticles and coupled with NiOOH to assemble into NiOOH/Cu interfacial structure.

The CO $_2$ RR catalytic activity of in situ formed NiOOH/Cu electrocatalysts was evaluated in a conventional three-electrode flow cell system using 1 m KOH as the electrolyte (refer to Experimental Section). The product FEs of the NiOOH/Cu electrocatalyst were determined at different current densities ranging from 100 to 500 mA cm $^{-2}$ (Figure 3a). It can be found that C $_2$ H $_4$ is the major CO $_2$ RR product at all current densities. The highest FE for C $_2$ H $_4$ reached 54.6 \pm 0.5% and the total FE of C $_2$ + products reached 86.3 \pm 3.0% at 400 mA cm $^{-2}$. The NiOOH/Cu electrocatalyst consistently exhibited high selectivity toward C $_2$ + products

(FEs > 75%) across all applied current densities, with a minor presence of H_2 (FE < 10%) and C_1 products (FEs < 13%). The corresponding applied potentials at different current densities are presented in Figure S11 (Supporting Information).

To investigate the impact of the Ni/Cu atomic ratio on electrocatalytic performance, we synthesized a series of NiOOH/Cu electrocatalysts with various Ni/Cu atomic ratios from 5% to 30% (denoted as NiOOH/Cu-X, where X represents the Ni/Cu atomic ratio). Inductively coupled plasma atomic emission spectroscopy (ICP-AES) was used to quantify the Ni/Cu atomic ratios (Table S4, Supporting Information). The NiOOH/Cu electrocatalysts with different atomic ratios have similar properties in morphology and valence state (Figures S12–S15, Supporting Information). However, we found a strong correlation between the Ni/Cu atomic ratio and $\rm C_{2+}$ products (Figure 3b; Figure S16, Supporting

1614649, 2024. 25, Downloaded from https://aba.acecd.onlinebitary.wiley.com/doi/10.1002/acmm.202400827 by Zhenxing Feng - Oregon State University, Wiley Online Library on [07/07/2025]. See the Terms and Conditions (https://onlinebitary.wiley.com/erms-and-conditions) on Wiley Online Library for rules of use; OA articles are governed by the applicable Creative Commons Licensea

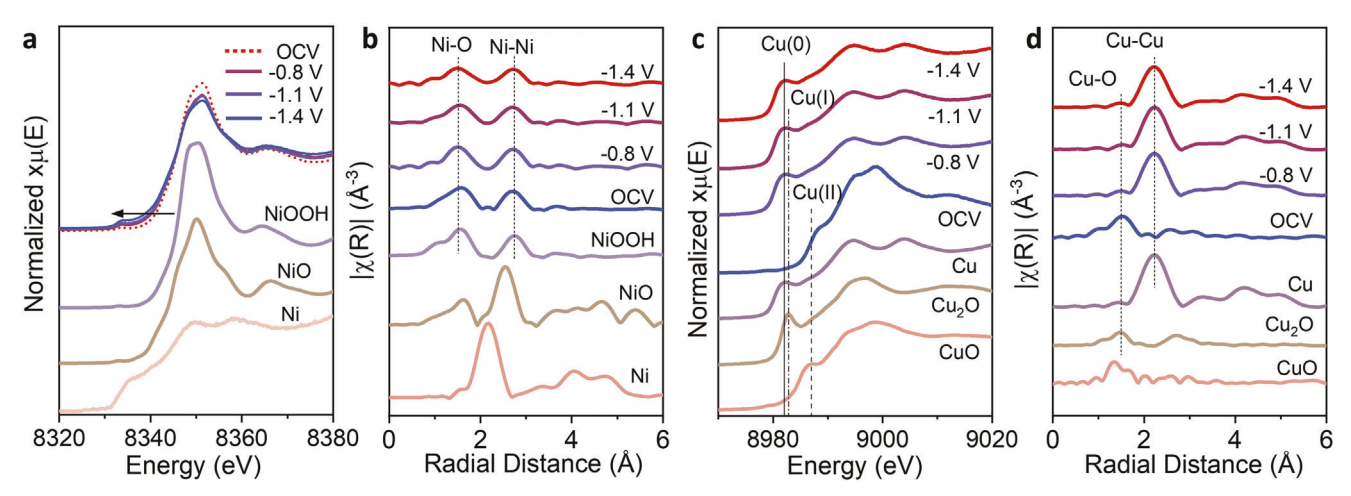


Figure 2. In situ XAS characterizations of the formation process of the NiOOH/Cu electrocatalyst. a) In situ Ni K-edge XANES spectra at OCV (NiCu-OP) and different reduction potentials. b) Fourier transform of the k^2 -weighted EXAFS spectra at Ni K-edge and corresponding fitting curves. The Ni K-edge EXAFS spectra of Ni, NiO, and β-NiOOH standards are included for comparison. c) In situ Cu K-edge XANES spectra of the NiOOH/Cu electrocatalyst and the Cu, Cu₂O, and CuO standards. d) Fourier transform of the k^2 -weighted EXAFS spectra at Cu K-edge and corresponding fitting curves. All in situ XAS measurements were performed in 1 M KOH.

Information). The electrochemical tests were performed at a constant current density of 400 mA cm⁻². The C₂₊ FE reveals a volcano relationship with different Ni/Cu atomic ratios. As the Ni/Cu atomic ratio decreased from 30% to 10%, the total FEs of C₂₊ products gradually increased from 37.1% to 86.3%, whereas the H₂ FE decreased progressively from 34.7% to 7.1%. This should be caused by the NiOOH cluster aggregation at higher contents increased HER activity. Furthermore, reducing the Ni/Cu atomic ratio from 10% to 5% also resulted in a decreased C2+ FE, due to diminished interfacial density, consequently influencing the electrocatalytic activity. In stark contrast, the bare Cu sample prepared using a similar method exhibited significantly decreased FEs toward C2+ products at all evaluated currents (Figure S17, Supporting Information). Specifically, the NiOOH/Cu-10 electrocatalyst exhibited a two-fold increase in C₂₊ product selectivity compared to the bare Cu at the current density of 400 mA cm $^{-2}$, but H $_2$ and CO FEs were significantly reduced (Figure 3c), which indicated that the present of NiOOH/Cu interfaces facilitates the formation of C_{2+} products.

To obtain further evidence for the role of the NiOOH/Cu interfaces in CO₂RR, we prepared several control samples for comparison, including bare Cu, bare NiOOH, and mechanically mixed NiOOH and Cu (denoted as NiOOH/Cu-mixed). The NiOOH/Cu electrocatalyst reflected the highest selectivity for C2+ products (Figure 3d). In contrast, the bare NiOOH exhibited no activity of CO₂RR (Figure \$18a, Supporting Information), which agrees with previous reports that the inorganic nickel oxygenates favor HER.[17] Interestingly, the bare Cu and NiOOH/Cu-mixed showed similar C_{2+} selectivity $\approx 40\%$ (Figure 3d; Figures S17 and \$18b, Supporting Information), suggesting that simply mixing the two species cannot bring extra active sites for C—C coupling. SEM and TEM mapping images indicated that the mechanically mixed NiOOH and Cu are unevenly distributed with poor interfacial contact (Figures S19 and S20, Supporting Information). In comparison, in situ derived NiOOH/Cu electrocatalysts are rich in interfaces of NiOOH and Cu with substantially improved C2+ selectivity by \approx 50%. At the same time, the effect of catalyst surface roughness on the selectivity of C₂₊ products were excluded (Figure S21, Supporting Information). Therefore, it is confirmed that the NiOOH/Cu interfaces are active sites for C—C coupling.

Additionally, a chronopotentiometry test was performed to evaluate the long-term stability of the NiOOH/Cu-10 electrocatalyst in a flow cell at 200 mA cm⁻² (Figure 3e; Figure S22, Supporting Information). Throughout the continuous 5-hour period of CO₂RR, the selectivity of C₂H₄ stays consistently above 50% with slight decay and the total FE of C₂₊ products remain above 70%. Competing HER was at a low level (H2 FE < 20%), which suggested that the NiOOH phase does not aggregate during electrocatalysis. The mass loss of the electrocatalyst was less than 0.01% by detecting the dissolved element content in the electrolyte after electrocatalysis (Table S5, Supporting Information). These results indicated the high structural stability of the NiOOH/Cu electrocatalyst. SEM and HR-TEM images revealed that the morphology of the NiOOH/Cu-10 was still maintained after a longtime CO₂RR (Figures S23 and S24, Supporting Information), which solidly confirms the robustness of the NiOOH/Cu interfacial structure. The long-term stability test was limited by salt precipitation and flooding on gas diffusion electrodes. Overall, the interfacial NiOOH/Cu electrocatalysts exhibited superior selectivity and remarkable long-term stability for C2+ products. Furthermore, the electrocatalytic activity of the NiOOH/Cu interfaces for C₂₊ products were evaluated by a gravitational current density based on the loading mass of active materials. Compared with the state-of-the-art catalysts, the NiOOH/Cu-10 electrocatalyst achieved the highest partial current density of 2085 A g⁻¹ for C_{2+} products (Figure 3f), which further demonstrated that the NiOOH/Cu interfaces possess extraordinarily high activity for C—C coupling.

It is well-known that CO_2RR to C_{2+} products undergoes a critical CO dimerization step, and a high CO coverage favors the C—C coupling reaction and inhibits the activity of the competing HER. [18] Therefore, we compared the coverage of surface-adsorb CO (*CO) on the NiOOH/Cu-10, Cu, and NiOOH electrocatalysts by in situ surface-enhanced Raman spectroscopy measurements

16146840, 2024, 25, Downloaded from https://advanced.onlinelibrary.wiley.com/doi/10.1002/aenm.202400827 by Zhenxing Feng - Oregon State University , Wiley Online Library on [07/07/2025]. See the Terms

ons) on Wiley Online Library for rules of use; OA articles are governed by the applicable Creative Commons License

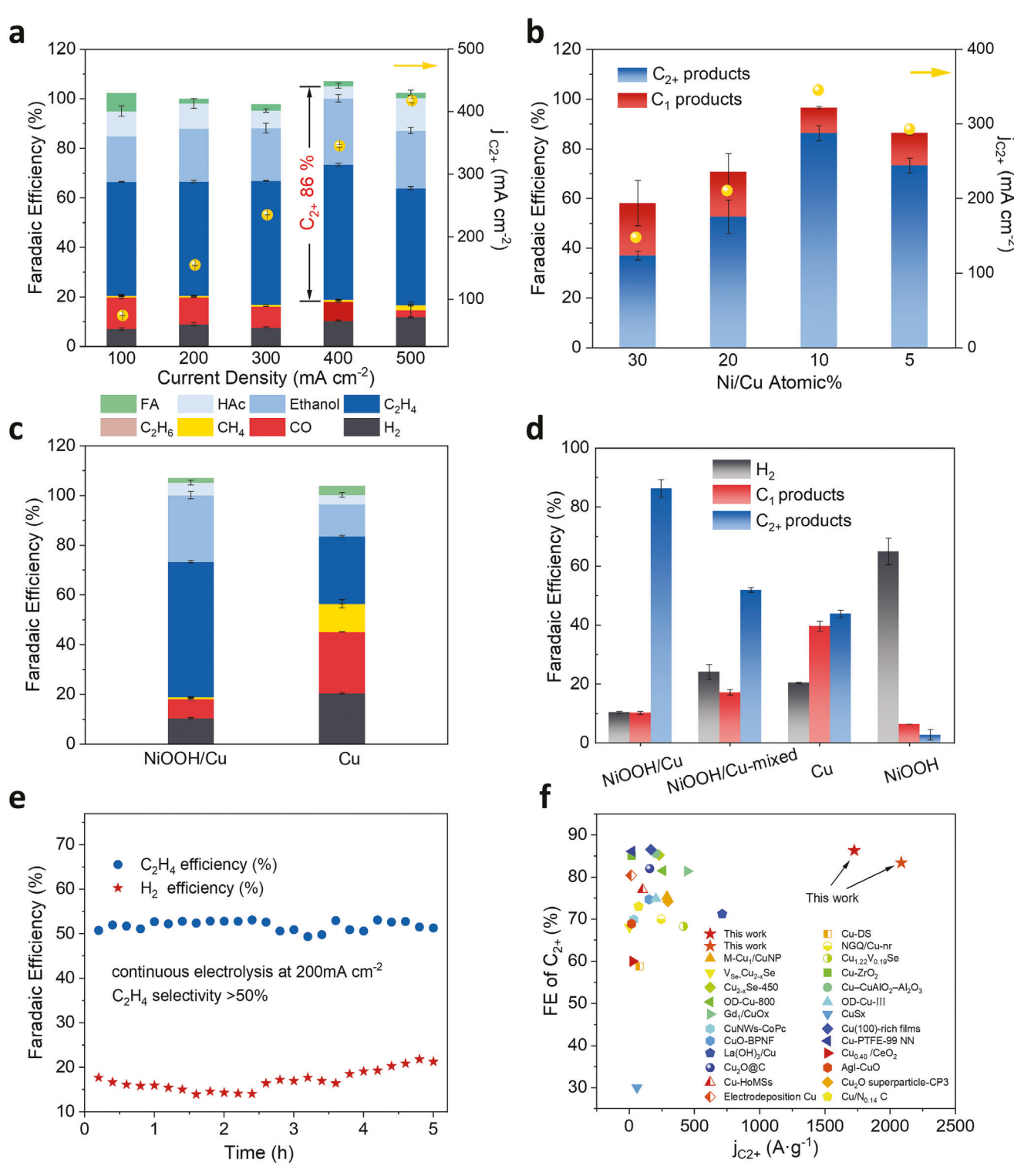


Figure 3. CO_2RR performance over NiOOH/Cu electrocatalysts. a) FEs of all the products under different geometrical current densities on the NiOOH/Cu-10 electrocatalyst. b) FEs of C_1 and C_{2+} products and j_{C2+} on the NiOOH/Cu-X samples with various Ni/Cu atomic ratios at a total current density of 400 mA cm⁻². c) FEs of all the products on the NiOOH/Cu-10 and bare Cu electrocatalysts at 400 mA cm⁻². d) Comparison of FEs of C_1 and C_{2+} products on the NiOOH/Cu-10, NiOOH-Cu mixed, Cu and NiOOH electrocatalysts at 400 mA cm⁻². e) Stability test of the NiOOH/Cu-10 at 200 mA cm⁻² in a flow cell along with the corresponding C_2 and C_2 and C_3 and C_4 and

16146840, 2024. 25, Downloaded from https://advanced.onlinelibrary.wiley.com/doi/10.1002/aemm.202400827 by Zhenxing Feng - Oregon State University , Wiley Online Library on [07/07/2025]. See the Terms and Conditions (https://onlinelibrary.wiley.com/doi/10.1002/aemm.202400827 by Zhenxing Feng - Oregon State University , Wiley Online Library on [07/07/2025]. See the Terms and Conditions (https://onlinelibrary.wiley.com/doi/10.1002/aemm.202400827 by Zhenxing Feng - Oregon State University , Wiley Online Library on [07/07/2025]. See the Terms and Conditions (https://onlinelibrary.wiley.com/doi/10.1002/aemm.202400827 by Zhenxing Feng - Oregon State University , Wiley Online Library on [07/07/2025]. See the Terms and Conditions (https://onlinelibrary.wiley.com/doi/10.1002/aemm.202400827 by Zhenxing Feng - Oregon State University , Wiley Online Library on [07/07/2025]. See the Terms and Conditions (https://onlinelibrary.wiley.com/doi/10.1002/aemm.202400827 by Zhenxing Feng - Oregon State University , Wiley Online Library on [07/07/2025].

nditions) on Wiley Online Library for rules of use; OA articles are governed by the applicable Creative Commons

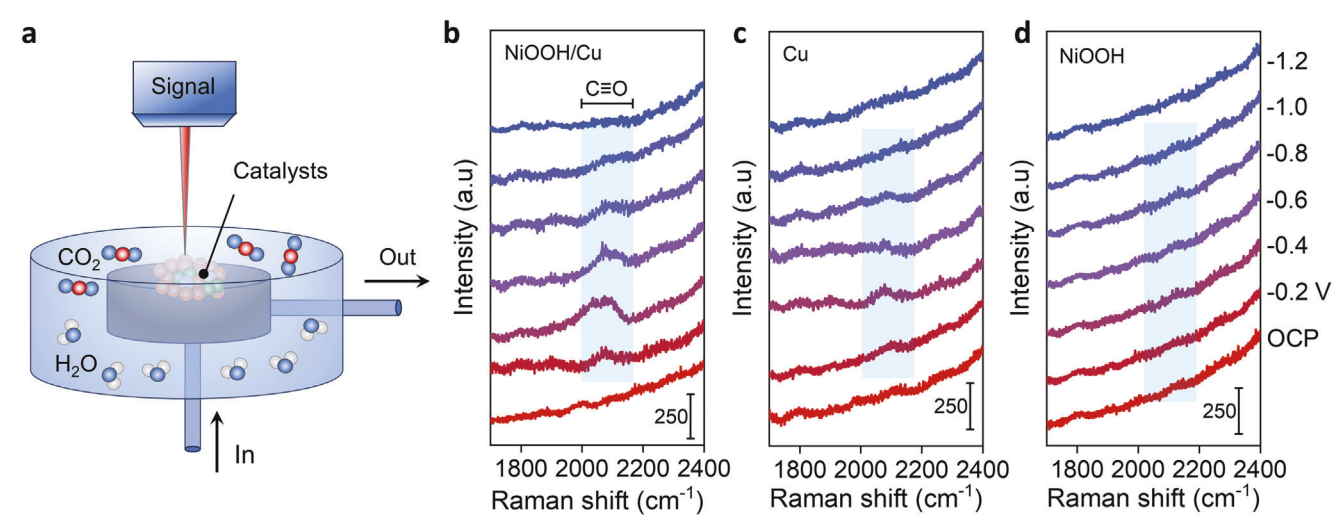


Figure 4. In situ surface-enhanced Raman spectroscopic studies. a) an Operando electrochemical flow cell with Raman spectra. b–d) In situ surface-enhanced Raman spectra in the region of 1800–2400 cm⁻¹ on b) NiOOH/Cu-10, c) Cu, and d) NiOOH catalysts in CO₂-saturated 0.1 м KHCO₃ at various potentials.

under cathodic potentials from −0.2 to −1.2 V versus RHE, respectively (**Figure 4**). The C≡O stretching mode near 2070 cm⁻¹ of the three electrocatalysts displayed notable differences. [16p] The NiOOH/Cu electrocatalyst showed the most obvious *CO signals (Figure 4b), meanwhile, its signals of Cu-CO stretching and frustrated rotation modes located at 280 and 360 cm⁻¹ were also observed (Figure S25, Supporting Information).[16p,19] In comparison, the peaks near 2070 cm⁻¹ for the bare Cu surface were largely weakened under all working potentials (Figure 4c). No peak was found using the NiOOH surface (Figure 4d), which should be due to the fact that NiOOH is more prone to undergo HER than CO₂RR, agreeing with the electrochemical results and previous literature.^[20] The Raman results illustrated that the NiOOH/Cu interfaces exhibit significantly improved ability to adsorb *CO, which is expected to promote the *CO dimerization reaction.

To further clarify the promoting effect of the NiOOH/Cu interface on CO dimerization, density functional theory (DFT) calculations were performed on the NiOOH/Cu interface and Cu

surface. Two reaction pathways were primarily considered, including dimerization of *CO (*OCCO) as a key step in the formation of C_{2+} products, and hydrogenation of *CO (*COH) as a competitive reaction for methane production. The optimal configurations of all reaction intermediates are shown in Figures S26–S30 (Supporting Information). The NiOOH and reaction intermediates were located on the surface of Cu (111). Representative structures are shown in Figure 5a–d, and detailed calculation results are given in Table S6 (Supporting Information).

The Gibbs free energy changes of the 2*CO→*OCCO path for the bare Cu surface and NiOOH/Cu interface were calculated to be 0.79 eV and −1.165 eV, respectively (Figure 5e). The less energy barrier of *OCCO formation at the NiOOH/Cu interface indicated that the dimerization of *CO is more efficient than that on the bare Cu surface. From the DFT-optimized structure, it was found that the Ni atom exposed by defect-rich NiOOH forms a Ni—O bond with *CO and *OCCO intermediates at the NiOOH/Cu interface (Figure 5a; Figure \$25, Supporting Information), which provides favorable conditions for the subsequent

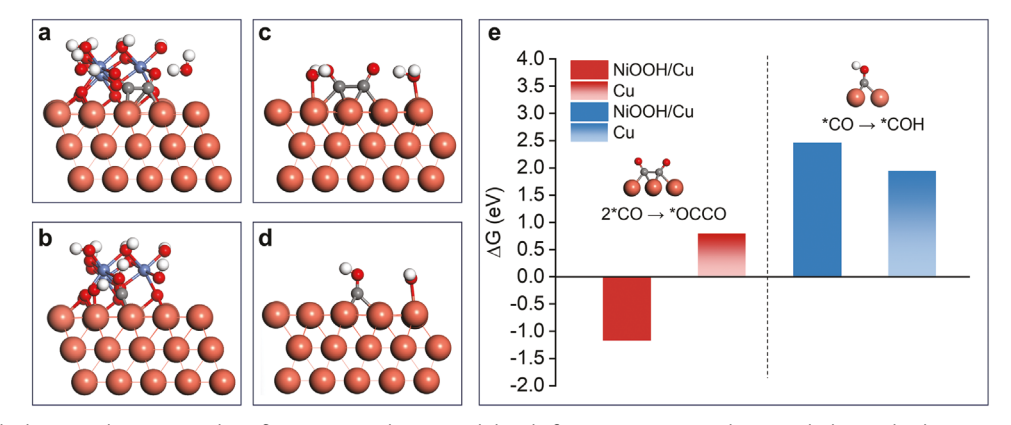


Figure 5. DFT calculations. The optimized configurations and structural details for *OCCO (a,c) and *COH (b,d) on a,b) the NiOOH/Cu interface and c,d) the Cu surface. e) Comparison of the Gibbs free energy changes of 2*CO to *OCCO and *CO to *COH reactions. The Ni, Cu, C, O, and H atoms are denoted by blue, brown, gray, red, and white balls, respectively.



C—C coupling reaction. The charge density map of *OCCO on the NiOOH/Cu interface further unveiled the synergy effect between the NiOOH and Cu (Figure S31, Supporting Information). Specifically, the positively charged center atom Ni polarizes the electron density of the terminal oxygen and the resulting overhanging carbon center is stabilized by the surface Cu atom, which provides the dual sites to stabilize *OCCO intermediates. Therefore, the NiOOH/Cu electrocatalyst with favorable interfacial electronic structure enhances the *CO adsorption and reduces the activation energy barrier of CO—CO dimerization.

Since the conversion of ${}^*\!\text{CO}$ to ${}^*\!\text{COH}$ via ${}^*\!\text{CO}$ hydrogenation will deplete ${}^*\!\text{CO}$ and disrupt the C_{2+} pathway, it should also be considered as the primary competitive reaction. The activation energy for the protonation of ${}^*\!\text{CO}$ to ${}^*\!\text{COH}$ at the NiOOH/Cu interface is significantly elevated by 0.52 eV compared to that on the bare Cu surface (Figure 5e), suggesting that the conversion of ${}^*\!\text{CO}$ to ${}^*\!\text{COH}$ is suppressed and thus the C_1 pathway is inhibited at the NiOOH/Cu interface. The energy barrier of ${}^*\!\text{CO}$ coupling is significantly lower than that of ${}^*\!\text{CO}$ protonation, verifying that the C_{2+} pathway is more advantageous for the NiOOH/Cu interface compared to the C_1 pathway.

3. Conclusion

We have successfully developed highly stable nickel oxygenate/Cu electrocatalysts with abundant NiOOH/Cu interfaces through an in situ electrochemical reconstruction. The interfacial electrocatalysts exhibit extraordinarily higher C2+ activity than the state-of-the-art electrocatalysts with a record partial current density of 2085 A g-1 and a superior Faradaic efficiency of 86.3 ± 3.0%, meanwhile, keep high structural stability during electrocatalysis. Combining in situ experimental and theoretical studies, we have discovered that the remarkable efficiency toward C₂₊ products is attributed to the in situ constructed highly dispersed NiOOH/Cu interfaces, which not only significantly increase the key intermediate *CO adsorption, but also provide dual sites for stabilizing the key intermediate *OCCO and lower the kinetic barrier for CO dimerization. Our work can provide a reference for constructing durable interfacial structures in various metal oxygenate/Cu electrocatalysts to achieve high selectivity for different products in CO₂RR.

Supporting Information

Supporting Information is available from the Wiley Online Library or from the author.

Acknowledgements

X.M., C.W.C., and. Z.L. contributed equally to this work. The authors gratefully appreciate the support of the National Natural Science Foundation of China (Nos. 51972223, 22109116, and 22309132), the National Key Research and Development Program of China (No. 2022YFB2404500), the National Industry-Education Integration Platform of Energy Storage, the Fundamental Research Funds for the Central Universities, and the Haihe Laboratory of Sustainable Chemical Transformations. Z. F., C.-W. C., and M. L. acknowledges the funding supports from the U.S. National Science Foundation (Nos. CBET-1949870 and CBET-2016192).

Conflict of Interest

The authors declare no conflict of interest.

Data Availability Statement

The data that support the findings of this study are available from the corresponding author upon reasonable request.

Keywords

copper, CO2 reduction, electrocatalysis, interface, reconstruction

Received: February 21, 2024 Revised: March 23, 2024 Published online: April 13, 2024 16146840, 2024, 25, Downloaded from https://abranced.onlinelbbrary.wiely.com/doi/10.1002/denm.20240827 by Zhenxing Feng - Organ State University, Wiley Online Library on [07/07/2025], See the Terms and Conditions (https://onlinelbbrary.wiely.com/terms-and-conditions) on Wiley Online Library for rules of use; OA articles are governed by the applicable Creative Commons License

- [1] M. Mostefaoui, P. Ciais, M. J. McGrath, P. Peylin, P. K. Patra, Y. Ernst, Earth Syst. Sci. Data. 2024, 16, 245.
- [2] L. Li, X. D. Li, Y. F. Sun, Y. Xie, Chem. Soc. Rev. 2022, 51, 1234.
- [3] a) S. Nitopi, E. Bertheussen, S. B. Scott, X. Liu, A. K. Engstfeld, S. Horch, B. Seger, I. E. L. Stephens, K. Chan, C. Hahn, J. K. Nørskov, T. F. Jaramillo, I. Chorkendorff, *Chem. Rev.* 2019, 119, 7610; b) Z. Yan, L. Xu, H. Zhu, *Renewables* 2023, 1, 278.
- [4] L. Xu, P. Trogadas, M.-O. Coppens, Adv. Energy Mater. 2023, 13, 2302974.
- [5] D. Raciti, C. Wang, ACS Energy Lett. 2018, 3, 1545.
- [6] a) X. Li, Q. Liu, J. Wang, D. Meng, Y. Shu, X. Lv, B. Zhao, H. Yang, T. Cheng, Q. Gao, L. Li, H. B. Wu, Chem 2022, 8, 2148; b) J. Li, A. Ozden, M. Wan, Y. Hu, F. Li, Y. Wang, R. R. Zamani, D. Ren, Z. Wang, Y. Xu, D. H. Nam, J. Wicks, B. Chen, X. Wang, M. Luo, M. Graetzel, F. Che, E. H. Sargent, D. Sinton, Nat. Commun. 2021, 12, 2808; c) S. Yan, Z. Chen, Y. Chen, C. Peng, X. Ma, X. Lv, Z. Qiu, Y. Yang, Y. Yang, M. Kuang, X. Xu, G. Zheng, J. Am. Chem. Soc. 2023, 145, 26374.
- [7] a) A. Vasileff, C. Xu, Y. Jiao, Y. Zheng, S.-Z. Qiao, Chem 2018, 4, 1809;
 b) M. Li, Y. Hu, T. Wu, A. Sumboja, D. Geng, Mater 2023, 67, 320.
- [8] a) A. Bagger, W. Ju, A. S. Varela, P. Strasser, J. Rossmeisl, ChemPhysChem 2017, 18, 3266; b) K. P. Kuhl, T. Hatsukade, E. R. Cave, D. N. Abram, J. Kibsgaard, T. F. Jaramillo, J. Am. Chem. Soc. 2014, 136, 14107.
- [9] a) X. Zhang, C. Liu, Y. Zhao, L. Li, Y. Chen, F. Raziq, L. Qiao, S.-X. Guo, C. Wang, G. G. Wallace, A. M. Bond, J. Zhang, Appl. Catal. B Environ. 2021, 291, 120030; b) H. Song, Y. C. Tan, B. Kim, S. Ringe, J. Oh, ACS Appl. Mater. 2021, 13, 55272.
- [10] S. Li, P. Ma, C. Gao, L. Liu, X. Wang, M. Shakouri, R. Chernikov, K. Wang, D. Liu, R. Ma, J. Wang, Energ Environ Sci 2022, 15, 3004.
- [11] a) Y. Zhou, A. J. Martín, F. Dattila, S. Xi, N. López, J. Pérez-Ramírez, B. S. Yeo, Nat. Catal. 2022, 5, 545; b) D. A. Torelli, S. A. Francis, J. C. Crompton, A. Javier, J. R. Thompson, B. S. Brunschwig, M. P. Soriaga, N. S. Lewis, ACS Catal. 2016, 6, 2100; c) K. U. D. Calvinho, A. B. Laursen, K. M. K. Yap, T. A. Goetjen, S. Hwang, N. Murali, B. Mejia-Sosa, A. Lubarski, K. M. Teeluck, E. S. Hall, E. Garfunkel, M. Greenblatt, G. C. Dismukes, Energ Environ Sci 2018, 11, 2550.
- [12] a) H. Cui, J. Xue, W. Ren, M. Wang, J. Nanopart. Res. 2014, 16, 2601;
 b) D. Y. Nadargi, M. S. Tamboli, S. S. Patil, R. B. Dateer, I. S. Mulla, H. Choi, S. S. Suryavanshi, ACS Omega 2020, 5, 8587.
- [13] a) Y.-F. Li, J.-L. Li, Z.-P. Liu, J. Phys. Chem. C 2021, 125, 27033; b) M. Cai, Q. Zhu, X. Wang, Z. Shao, L. Yao, H. Zeng, X. Wu, J. Chen, K. Huang, S. Feng, Adv. Mater. 2023, 35, 2209338.
- [14] P. Tan, Y. Wu, Y. Tan, Y. Xiang, L. Zhou, N. Han, Y. Jiang, S. J. Bao, X. Zhang, Small 2023, 2308371. https://doi.org/10.1002/smll. 202308371

16146840, 2024, 25, Downloaded from https://advanced.onlinelibrary.wiley.com/doi/10.1002/nemm.202400827 by Zhaxing Feng - Oregon State University , Wiley Online Library on [07/07/2025]. See the Terms and Conditions (https://onlinelibrary.

com/terms-and-conditions) on Wiley Online Library

for rules of use; OA articles are governed by the applicable Creative Commons License

www.advancedsciencenews.com

www.advenergymat.de

- [15] a) M. Wang, L. Árnadóttir, Z. J. Xu, Z. Feng, Nanomicro Lett 2019, 11, 47; b) M. Wang, Z. Feng, Curr. Opin. Electrochem. 2021, 30, 100803;
 c) Z. Weng, Y. Wu, M. Wang, J. Jiang, K. Yang, S. Huo, X.-F. Wang, Q. Ma, G. W. Brudvig, V. S. Batista, Y. Liang, Z. Feng, H. Wang, Nat. Commun. 2018, 9, 415.
- [16] a) J. Feng, L. Zhang, S. Liu, L. Xu, X. Ma, X. Tan, L. Wu, Q. Qian, T. Wu, J. Zhang, X. Sun, B. Han, Nat. Commun. 2023, 14, 4615; b) H. Wang, X. Bi, Y. Yan, Y. Zhao, Z. Yang, H. Ning, M. Wu, Adv. Funct. Mater. 2023, 33, 2214946; c) K. Lakshmanan, W. H. Huang, S. A. Chala, C. Y. Chang, S. T. Saravanan, B. W. Taklu, E. A. Moges, Y. Nikodimos, B. D. Dandena, S. C. Yang, J. F. Lee, P. Y. Huang, Y. C. Lee, M. C. Tsai, W. N. Su, B. J. Hwang, Small 2023, 2307180; https://doi.org/10.1002/ smll.202307180 d) C. Li, Z. Guo, Z. Liu, T. Zhang, H. Shi, J. Cui, M. Zhu, L. Zhang, H. Li, H. Li, C. Li, ACS Catal. 2023, 13, 16114; e) J. Feng, L. Wu, S. Liu, L. Xu, X. Song, L. Zhang, Q. Zhu, X. Kang, X. Sun, B. Han, J. Am. Chem. Soc. 2023, 145, 9857; f) Y. Luo, J. Yang, J. Qin, K. Miao, D. Xiang, A. Kuchkaev, D. Yakhvarov, C. Hu, X. Kang, J. Energy Chem. 2024, 92, 499; g) F. Pan, X. Duan, L. Fang, H. Li, Z. Xu, Y. Wang, T. Wang, T. Li, Z. Duan, K.-J. Chen, Adv. Energy Mater. 2023, 14, 2303118; h) S. Hu, Y. Chen, Z. Zhang, S. Li, H. Liu, X. Kang, J. Liu, S. Ge, J. Wang, W. Lv, Z. Zeng, X. Zou, Q. Yu, B. Liu, Small 2023, 20, 2308226; i) Y. Zang, T. Liu, P. Wei, H. Li, Q. Wang, G. Wang, X. Bao, Angew. Chem., Int. Ed. 2022, 61, 202209629; j) C. Liu, M. Zhang, J. Li, W. Xue, T. Zheng, C. Xia, J. Zeng, Angew. Chem., Int. Ed. 2022, 61, 202113498; k) X. Zhang, J. Li, Y.-Y. Li, Y. Jung, Y. Kuang, G. Zhu, Y. Liang, H. Dai, J. Am. Chem. Soc. 2021, 143, 3245; l) Z. Gu, H. Shen, Z. Chen, Y. Yang, C. Yang, Y. Ji, Y. Wang, C. Zhu, J. Liu, J. Li, T.-K. Sham, X. Xu, G. Zheng, Joule 2021, 5, 429; m) C. Chen, X. Yan, S. Liu, Y. Wu, Q. Wan, X. Sun, Q. Zhu, H. Liu, J. Ma, L. Zheng, H. Wu, B. Han, Angew. Chem., Int. Ed. 2020, 59, 16459; n) W. Sun, P. Wang, Y. Jiang, Z. Jiang, R. Long, Z. Chen, P. Song, T. Sheng, Z. Wu, Y. Xiong, Adv. Mater. 2022, 34, 2207691; o) X. Wang, Y. Jiang, K. Mao, W. Gong, D. Duan, J. Ma, Y. Zhong, J. Li, H. Liu, R. Long, Y. Xiong, J. Am. Chem. Soc. 2022, 144, 22759; p) Z.-Z. Wu, X.-L. Zhang, Z.-Z. Niu, F.-Y. Gao,
- P.-P. Yang, L.-P. Chi, L. Shi, W.-S. Wei, R. Liu, Z. Chen, S. Hu, X. Zheng, M.-R. Gao, J. Am. Chem. Soc. 2022, 144, 259; q) C. Peng, G. Luo, J. Zhang, M. Chen, Z. Wang, T.-K. Sham, L. Zhang, Y. Li, G. Zheng, Nat. Commun. 2021, 12, 1580; r) G. Zhang, Z.-J. Zhao, D. Cheng, H. Li, J. Yu, Q. Wang, H. Gao, J. Guo, H. Wang, G. A. Ozin, T. Wang, J. Gong, Nat. Commun. 2021, 12, 5745; s) B. Yang, K. Liu, H. Li, C. Liu, J. Fu, H. Li, J. E. Huang, P. Ou, T. Alkayyali, C. Cai, Y. Duan, H. Liu, P. An, N. Zhang, W. Li, X. Qiu, C. Jia, J. Hu, L. Chai, Z. Lin, Y. Gao, M. Miyauchi, E. Cortés, S. A. Maier, M. Liu, J. Am. Chem. Soc. 2022, 144, 3039; t) J. Yin, Z. Gao, F. Wei, C. Liu, J. Gong, J. Li, W. Li, L. Xiao, G. Wang, J. Lu, L. Zhuang, ACS Catal. 2022, 12, 1004; u) R. Yang, J. Duan, P. Dong, Q. Wen, M. Wu, Y. Liu, Y. Liu, H. Li, T. Zhai, Angew. Chem., Int. Ed. 2022, 61, 202116706; v) Y. Jiang, X. Wang, D. Duan, C. He, J. Ma, W. Zhang, H. Liu, R. Long, Z. Li, T. Kong, X. J. Loh, L. Song, E. Ye, Y. Xiong, Adv. Sci. 2022, 9, 2105292; w) X. Su, Z. Jiang, J. Zhou, H. Liu, D. Zhou, H. Shang, X. Ni, Z. Peng, F. Yang, W. Chen, Z. Qi, D. Wang, Y. Wang, Nat. Commun. 2022, 13, 1322.
- [17] a) N. Farahbakhsh, S. Sanjabi, J. Ind. Eng. Chem. 2019, 70, 211; b) S. Lu, B. Zhao, M. Chen, L. Wang, X.-Z. Fu, J.-L. Luo, Int. J. Hydrogen Energy 2021, 46, 1540.
- [18] a) D. Zhong, Z. J. Zhao, Q. Zhao, D. Cheng, B. Liu, G. Zhang, W. Deng, H. Dong, L. Zhang, J. Li, J. Li, J. Gong, Angew. Chem., Int. Ed. 2021, 60, 4879; b) P. De Luna, R. Quintero-Bermudez, C.-T. Dinh, M. B. Ross, O. S. Bushuyev, P. Todorović, T. Regier, S. O. Kelley, P. Yang, E. H. Sargent, Nat. Catal. 2018, 1, 103; c) Y. Chen, N. Lyu, J. Zhang, S. Yan, C. Peng, C. Yang, X. Lv, C. Hu, M. Kuang, G. Zheng, Small 2023, 2308004. https://doi.org/10.1002/smll.202308004
- [19] S. Jiang, K. Klingan, C. Pasquini, H. Dau, J. Chem. Phys. 2019, 150, 041718.
- [20] a) Z. Qiu, Y. Ma, T. Edvinsson, Nano Energy 2019, 66, 104118; b) Y. Pei, L. Huang, L. Han, H. Zhang, L. Dong, Q. Jia, S. Zhang, Green Energy Environ. 2022, 7, 467.
- [21] C. Peng, X. Zhu, Z. Xu, S. Yan, L. Y. Chang, Z. Wang, J. Zhang, M. Chen, T. K. Sham, Y. Li, G. Zheng, Small 2022, 18, 2106433.